MOEM

Modern Electronic Materials 4(4): 151–162
DOI 10.3897/j.moem.4.4.35062

Research Article

Synthesis and characterization of N, O-donor Schiff base capped ZnS NPs as a sensor for fluorescence selective detection of Fe^{3+}, Cr^{2+} and Cd^{2+} ions

Dasari Ayodhya[1], Guttena Veerabhadram[1]

1 Department of Chemistry, Osmania University, Hyderabad, Telangana State-500007, India

Corresponding author: *Guttena Veerabhadram* (gvbhadram@osmania.ac.in)

Received 2 April 2018 ♦ **Accepted** 3 August 2018 ♦ **Published** 1 December 2018

Citation: Ayodhya D, Veerabhadram G (2018) Synthesis and characterization of N, O-donor Schiff base capped ZnS NPs as a sensor for fluorescence selective detection of Fe^{3+}, Cr^{2+} and Cd^{2+} ions. Modern Electronic Materials 4(4): 151–162. https://doi.org/10.3897/j.moem.4.4.35062

Abstract

We report the simple synthesis of zinc sulfide nanoparticles (ZnS NPs) by a co-precipitation method using Schiff base, (2-[(4-methoxy-phenylimino)-methyl]-4-nitro phenol) as a capping agent. Here, Schiff base is also used as N, O-donor ligand to control the morphology of NPs and fluorescence interactions. The formation of ZnS NPs and their optical, structural, thermal properties and morphologies were studied by means of UV–vis DRS, fluorescence, FTIR, XRD, SEM, TEM, zeta potential and TGA. The optical properties and quantum confinement effect of the products were confirmed by means of spectroscopic measurements. XRD and TEM image shows that the synthesized ZnS NPs have cubic structures with a diameter of about less than 10 nm. The prepared ZnS NPs exhibited as a selective probe detection of Fe^{3+}, Cr^{2+} and Cd^{2+} ions by fluorometrically and the emission band which disappears in the presence of increasing concentrations of Fe^{3+}, Cr^{2+} and Cd^{2+} ions. Based on the fluorescence quenching of the NPs in the presence of metal ion of interest, the feasibility of their determinations was examined according to the Stern-Volmer equation. Our work suggested that Schiff base capped ZnS NPs could be a potential selective sensor in the detection of heavy metal ions.

Keywords

ZnS NPs, schiff base, fluorescence sensor, selective probe, metal ion detection

1. Introduction

Nanostructure-based semiconductor materials are of great importance for several technological applications due to their optical and thermal properties. The design and fabrication of metal sulfide nanoparticles with tunable properties for advanced applications have drawn a great deal of attention in the field of nanotechnology due to the quantum size and surface effects. These unique properties make them suitable for many applications. Wide direct band gap semiconductor materials like ZnS have gained special notice due to their size-dependent properties and widespread technological applications. The semiconductor-based NPs and composites such as ZnS, CdS, CdSe, CdS/Fe_3O_4, CdS/TiO_2, $CdIn_2S_4$, Ag_2S, Ag_2S/SiO_2, Ag_2S/TiO_2, Bi_2S_3, NiS, CoS, CuS, HgS and PbS with varied band gap have been studied due to their wide use in optoelectronics, electronics, light-emitting diodes, electroluminescence, flat panel displays, infrared windows, sensors, lasers, bio-devices and catalytic applications

[1–13]. In II–VI semiconductor NPs, ZnS is considered an important material due to its structural stability with potential applications in optoelectronics, luminescence, photocatalysis, displays, sensors, and absorption studies [14–17]. It is known that bulk ZnS is an important binary semiconductor with a direct, wide band gap (~3.6 eV), high refraction index, and high transmittance in the visible range [18].

In recent years, many methods have been developed to prepare semiconductor NPs using physical and chemical techniques. Physical methods such as liquid microwave irradiation [19], reverse micelles [20], chemical vapor deposition [21], solid-liquid chemical reactions under co-precipitation [22], and hydrothermal techniques [23] have been used to synthesize ZnS NPs. These metal sulfide materials have tremendous luminescence activity with wide band gaps has been investigated for a long time [24], because, these measurements yield information about the energetic positions of the electronic states in the gap [25]. ZnS is an important luminescence material with a wide band gap, widely used in fluorescence applications. In addition, many works have explored the luminescence properties of ZnS NPs, with various experimental methods: photoluminescence [26], thermo-luminescence [27], electro-luminescence [28], optical absorption [29] and so on. In spite of this, the processes involved in luminescence are still not very clear. The use of semiconductors as fluorescence probes has increased in recent years along with their applications in different areas such as medicine, chemistry, and engineering. This interest is related to their broad absorption spectra and strong and tunable fluorescence [3–6].

Development of novel fluorescent sensors has attracted significant interest for selective and sensitive detection of metal ions in environmental and biological samples [30–31]. In the recent years, semiconductor nanoparticles or quantum dots **(QDs)** have developed as luminescent probes for sensing events [16]. In the case of semiconductor nanoparticles, ZnS NPs, with wide band gap energy is particularly suitable for the sensing and detection of heavy metal ions. Presently, the development of modern industry, agriculture and transport, heavy metal pollution has become increasingly serious and an important aspect of environmental pollution. Heavy metal pollution is wide-ranging contamination with long duration and is difficult to eliminate due to its persistent characteristic in biological material recycling and energy exchange, resulting in the transmission and enrichment of heavy metal through food chains ultimately endangering human health.

In the aspect of environmental pollution includes various heavy ions such as cations (Pb^{2+}, Cd^{2+}, Hg^{2+}, Fe^{3+}, Cr^{2+} and Cu^{2+} etc.) and anions (X^-, IO_3^-, ClO_4^-, NO_2^-, S_2^-, CN^- and N_3^- etc.) in different media was harmful to the environment as well as human health. Therefore, the detection of heavy ions is owing to their biological importance or environmental harm, have attracted more and more attention. There are many kinds of qualitative and quantitative methods for detection of various cations and anions in different media, using various techniques such as titrimetry, voltammetry, flow-injection analysis, inductively coupled plasma atomic emission spectroscopy, electrochemical methods, chromatography, chemiluminescence, colorimetry and fluorescence spectrometry [32–38]. Among the various reported techniques, fluorescent sensors present many appealing advantages, including high sensitivity, low cost, easy detection, and remote control. Many of these methods suffer from the need for extensive sample manipulation, subtraction of large numbers from each other, and relevant analysis time [39–40]. However, among the metal ions, iron, cadmium and chromium; and solutions of its compounds are extremely toxic even in low concentrations, because the excess amounts of Fe^{3+}, Cr^{2+} and Cd^{2+} ions can cause damage to cellular lipids, nucleic acids, and proteins. Furthermore, these heavy metal ions damaged to the liver and the kidney; and causes of the diabetes and heart disease. Therefore, the detection of Fe^{3+}, Cr^{2+} and Cd^{2+} ions has become a matter of considerable interest in environmental and biological samples.

Schiff bases, derived from the condensation of primary amines and aldehydes or ketones are characterized by the anil-linkage –HC=N–, possess structural similarities with natural biological substances. They have a wide variety of applications in biological, inorganic, clinical and analytical fields [41–42]. They are known to exhibit potent antimicrobial (antibacterial, antiviral and antifungal), anticonvulsant, anti-inflammatory and insecticidal activities [41–43]. In addition, some Schiff bases show pharmacologically useful activities like anti-cancer (radical scavenging activity), antihypertensive, anti-fertility, analgesic, anthelmintic, and hypnotic activities [43]. So far, however, the studies on the synthesis of nanosized structures with Schiff bases or Schiff base derived metal complexes as precursors have been less reported [3]. Especially, much fewer studies on the preparation of semiconductor NPs have been performed on different Schiff bases and their metal complexes. The way using Schiff bases as precursors may be helpful to manipulate the structure, purity, morphology, optical and luminescent properties of ZnS NPs.

We report in this paper, the synthesis of Schiff base capped ZnS NPs using a simple co-precipitation method. The prepared ZnS NPs were characterized by several physicochemical techniques such as UV–vis DRS, PL, FTIR, XRD, SEM, TEM, and TGA. The prepared ZnS NPs exhibited simple cubic structure with the average size of the NPs is about 10 nm. The synthesized ZnS NPs were used as fluorescent sensors for detection of metal ions such as Mn^{2+}, Ba^{2+}, Al^{3+}, Cd^{2+}, Cr^{2+}, Cu^{2+}, Fe^{3+}, Ni^{2+}, Co^{2+} and Ag^+. But Fe^{3+}, Cr^{2+} and Cd^{2+} metal ions caused a significant fluorescence quenching of ZnS NPs. The prepared ZnS NPs as selective probes for the detection of several heavy metal ions, especially Fe^{3+}, Cr^{2+} and Cd^{2+} in μM range of concentrations. Furthermore, the proposed NPs as sensors were employed for the determination of metal ions with satisfactory results.

2. Experimental

2.1. Materials and methods

Zinc acetate dihydrate, sodium sulfide, cadmium acetate, copper acetate, nickel acetate, chromium chloride and cobalt chloride chemicals were purchased from Sigma-Aldrich (97%, Bangalore Bonded Warehouse, India); manganese chloride, barium chloride and aluminium chloride were obtained from SD Fine-Chem Limited (Worli Road, Mumbai, India); ferric nitrate and silver nitrate were purchased from Finar Limited (Ellisbridge, Ahmedabad, India). Double distilled water was used throughout this experiment. All the reagents were analytical grade and used without further purification.

2.2. Synthesis of Schiff base capped ZnS NPs

ZnS NPs were synthesized by co-precipitation method by adding an equal amount of Zn^{2+} solution and S^{2-} as precipitating anion formed by decomposition of sodium sulfide nonahydrate. To prepare Schiff base capped ZnS NPs, 25 ml of 0.25 M zinc acetate and an equal quantity of 0.25 M sodium sulfide were dissolved separately in double distilled water. The solutions were stirred for 30 min using magnetic stirrer. The prepared 2-[(4-methoxy-phenylimino)-methyl]-4-nitrophenol was used as a capping agent to prevent agglomeration of ZnS NPs. In a separate beaker, 5×10^{-3} M of Schiff base was dissolved in 10 ml of methanol and was stirred. To the stirred solution of zinc acetate, a solution of Schiff base was poured drop by drop. After 30 min, the solution of sodium sulfide was poured drop by drop similarly. A very fine precipitate appeared soon after the addition of sodium sulfide. After formation of a white colored precipitate, the resulting ZnS precipitate was collected, filtered, washed with double distilled water and absolute ethanol several times to remove the unreacted chemicals, and finally dried in a furnace at 80 °C for 5 h. The probable reaction mechanism of formation of Schiff base capped ZnS NPs by the co-precipitation method is shown as follows in Fig. 1. Further, the nanoparticles were subjected to characterization for their morphology, stability and particle size.

2.3. Characterization techniques

X-ray diffraction **(XRD)** pattern was recorded on X'Pert PHILIPS, 30 kV, 40 mA using nickel-filtered CuKα radiations (λ = 1.5406 Å). The UV–vis diffuse reflectance spectra (UV–vis DRS) were recorded using a Shimadzu 3600 spectrophotometer in the spectral range of 200–800 nm. Transmission electron microscopy **(TEM)** was performed on TECNAI G2 and the microscope was operated at 200 kV. Samples were prepared by dispersing the powder in water. Imaging was recorded by depositing few drops of suspension on a carbon coated 400 mesh Cu grid. The solvent was left to evaporate before imaging. Scanning electron microscopy **(SEM)** images of fabricated ZnS NPs were obtained using ZEISS EVO18 electron microscope. Fourier transforms infrared **(FTIR)** spectra on KBr pellet were measured on a Shimadzu spectrophotometer in the range of 4000–400 cm^{-1}. The photoluminescence **(PL)** spectrum was measured with an RF–5301PC spectrofluorometer (Shimadzu, Japan). The thermal behavior and degradation of the ZnS NPs were investigated by thermogravimetric analysis **(TGA)** in the temperature range of 40 to 800 °C at a heating rate of 10 °C min^{-1}, under the nitrogen atmosphere. Zeta potential measurements were determined with the Zetasizer Nano ZS (Malvern Instruments, UK).

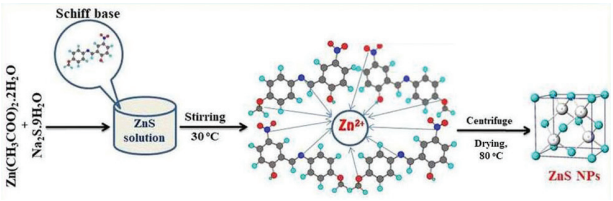

Figure 1. The possible schematic mechanism of the Schiff base capped ZnS NPs by co-precipitation method.

2.4. Fluorescence sensing procedure

Fluorescence spectroscopy studies were carried out in order to evaluate the ability of the receptors to operate as cation sensors. As most of the tested metal ions are highly toxic and have adverse effects on human health, all experiments involving heavy metal ions and other toxic chemicals were performed with protective gloves. The waste solutions containing heavy metal ions were collectively reclaimed to avoid polluting the environment. The nitrate, acetates and chloride salts of the metal (Mn^{2+}, Ba^{2+}, Al^{3+}, Cd^{2+}, Cr^{2+}, Cu^{2+}, Fe^{3+}, Ni^{2+}, Co^{2+} and Ag^{+}) were dissolved in double distilled water to prepare 1×10^{-3} M stock solutions. A solution of Schiff base capped ZnS NPs was prepared in double distilled water. Titration experiments were carried out in 1 cm quartz cuvette at room temperature. 2mL of ZnS NPs solution was placed in the quartz cell and the fluorescence spectrum was recorded. It was then titrated by successive additions in small portions (10 mL) of the solution of corresponding metal salt (1×10^{-6} M) and fluorescence intensity changes were recorded at room temperature. Various concentrations (10, 20, 30, 40, 50, 60, 70, 80, 90, 100, 200, 300, 400, 500 μM) of Fe^{3+}, Cr^{2+} and Cd^{2+} (0.5 ml) were added to the ZnS solution (2.5 ml) to test the sensitivity limits of Schiff base capped ZnS NPs. The mixtures were measured within seconds after adding metal ions by a fluorescence spectrophotometer (at λ_{em} = 430 nm, λ_{ex} = 340 nm).

3. Results and discussion

3.1. UV–vis DRS analysis

The optical methods take advantage of observing the essential characteristics of the nanomaterials without significant-

ly modifying or permanently damaging them due to their non-contact and non-invasive nature. Nanoparticles are ideal for ultrasensitive and multiple applications in optical sensing, so there is a need to explore the optical properties of these nanoparticles [44]. To understand the performance of semiconductor nanocrystals, the study of their optical absorption is important. The optical properties of the samples were studied by DRS in the UV–vis region. Fig. 2 shows the UV–vis DRS recorded at room temperature in the wavelength range of 200–800 nm. From this spectrum, it may be observed that the absorption edge of the synthesized ZnS NPs is slightly shifted to lower wavelength compared to the bulk ZnS. The absorption peak of the synthesized ZnS NPs appeared in the spectral range of 300–330 nm wavelength (311 nm, E_g = 3.98 eV). It showed a characteristic shift in the absorbance band edge to lower wavelength relevant to the bulk ZnS materials (345 nm, E_g = 3.6 eV) [45]. The interception of the tangent on the descending part of the absorption peak of the wavelength axis gives the value of diffuse absorption edge (nm). Band gap values were calculated from the following equation: $E_g = 1240/\lambda$, where λ is the wavelength of the absorption edge. The nature and the value of optical band gap can be determined from the fundamental absorption values, which corresponds to electron excitation from valence band to conduction band. This methodology was based on the transformation of diffuse reflectance measurements to estimate E_g from the Fig. 2; the band gap value obtained was 3.98 eV.

3.2. PL analysis

One of the most important optical properties of the ZnS NPs is their PL emission, which depends on the size, shape, and surface energetic states, which are further influenced by surface passivation [46]. PL spectrum is an effective tool to evaluate the defects and optical properties of ZnS NPs as a photonic material. Also, PL spectrum is sensitive to synthetic conditions, size, and shape of NPs. Broadening of the emission peak could be attributed to both size distribution and an increase in the surface states owing to the increase in surface to volume ratio for ZnS NPs [47]. From literature, it can be noticed that the PL of uncapped ZnS NPs shows only a broad peak between 350 and 550 nm [48]. Fig. 3 shows the PL spectra of ZnS NPs at an excitation wavelength of 340 nm and the emission peak is noted at 432 nm. This PL spectrum exhibits size-dependent quantum confinement effects with abroad peak at 432 nm indicating surface irregularity attributed to the presence of sulfur vacancies in the lattice [49]. Further, it can be incurred that the emissions correspond to the electron or holes hollow traps which act as recombination centers for photogenerated charge carriers and this phenomenon may be due to photo-oxidation process which occurs on the surface of ZnS NPs in the presence of UV light [50].

3.3. FTIR analysis

FTIR spectrum of the Schiff base capped ZnS NPs is shown in Fig. 4. In the FTIR spectrum of the ZnS NPs (Fig. 4), 3448, 1641, 1437 and 1141 cm^{-1} are assigned to O–H stretching in phenols, N=O stretching in nitro compounds, C–C stretching in aromatics, C–N stretching and C–O stretching respectively. Previously reported [3] that the characteristic peaks of Schiff base appear at 1516, 1641 and 1248 cm^{-1} corresponding to the absorptions of C=N, C=C, and C–O, which proves that the organic component is mainly Schiff base coordinated onto the ZnS NPs surface. The new weak bands observed at 874, 617 and 458 cm^{-1} which are not seen in the spectrum of Schiff base can be attributed to υ(Zn–O), υ(Zn–N) and υ(Zn–S). The wavenumbers of these characteristic peaks are higher than those appearing in Schiff base sample. This is probably because of the coordination bond between the Schiff base and zinc ions, which makes the vibration of the carbonyl and hydroxyl groups move to higher wavenumber. These results indicate that Schiff base plays an important role in enhancing the polydisperse nature of the nanoparticles by the formation of coordinate interactions between the Schiff base and the Zn^{2+} ions, thereby lowering their surface energies.

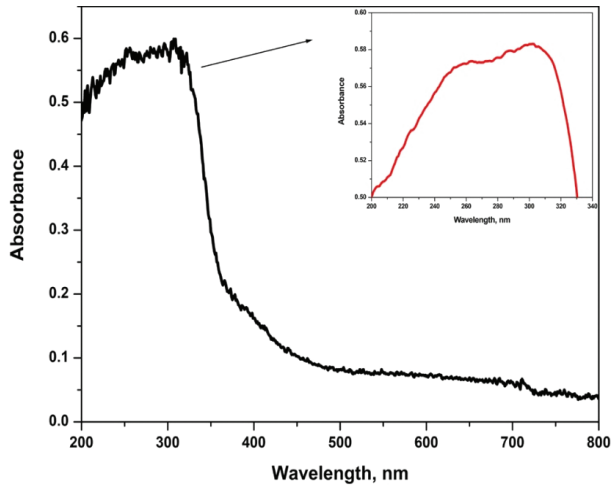

Figure 2. UV–vis DRS of Schiff base capped ZnS NPs.

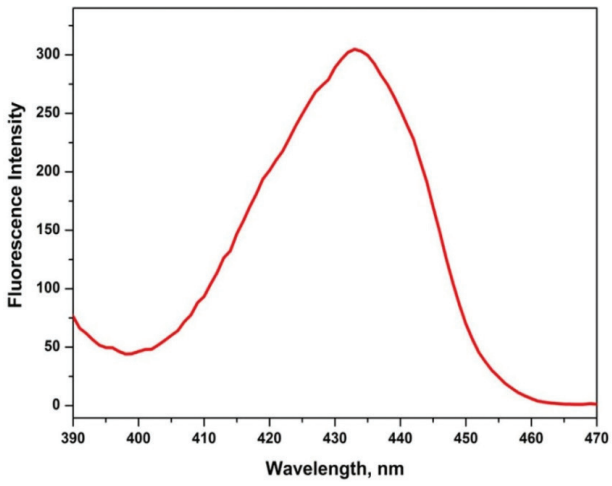

Figure 3. PL spectrum of Schiff base capped ZnS NPs.

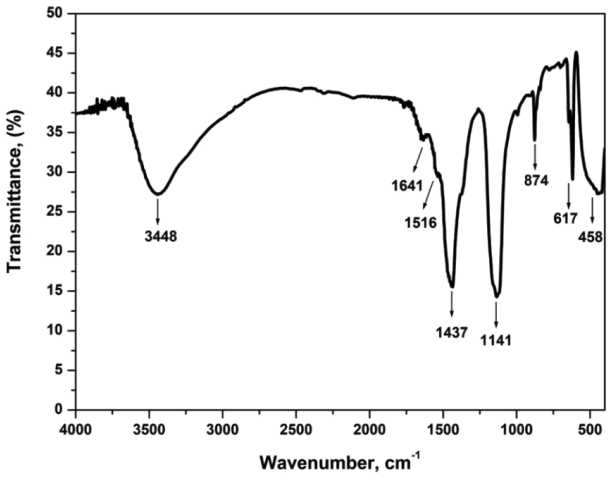

Figure 4. FTIR spectrum of Schiff base capped ZnS NPs.

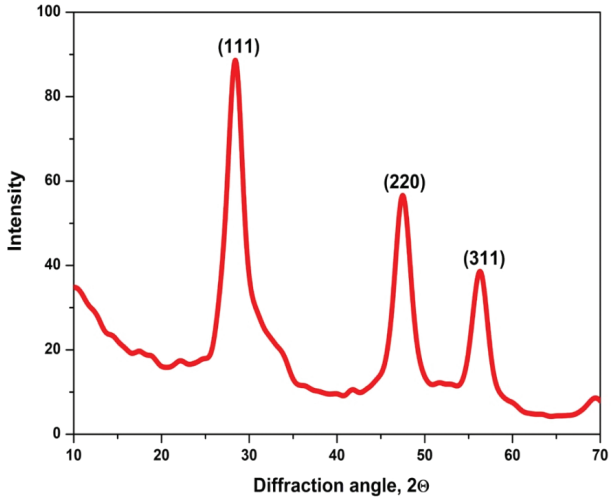

Figure 5. XRD spectrum of Schiff base capped ZnS NPs.

3.4. XRD analysis

XRD analysis was carried out to determine the crystalline nature of the Schiff base capped ZnS NPs and shown in Fig. 5. The diffraction peaks at 28.65, 47.56 and 56.44° correspond to (111), (220), and (311) planes of cubic ZnS (Fig. 5). The typical broadening of the diffraction peaks is also observed, implying that the size of the ZnS NPs is very small. XRD pattern of the Schiff base capped ZnS NPs confirms the crystallinity of the systems corresponding to cubic zinc blende (JCPDS 05–0566). The size of the ZnS NPs was calculated by following the Debye-Scherrer's equation:

$$D = \frac{k\lambda}{\beta\cos\theta}. \quad (1)$$

where $k = 0.95$, D is the particle size, λ is the wavelength of CuK_α radiation and β is the corrected full width at half maximum of the diffraction peak. From the XRD pattern, the observed size of the Schiff base capped ZnS NPs is 14 nm at the high intense peak of (111) plane. The lattice parameters are calculated by the formula:

$$1/d^2 = 1/a^2(h^2 + k^2 + l^2),$$

where a is lattice parameter, d_{hkl} is the interplanar separation corresponding to Miller indices (h, k and l). The estimated value of the lattice constant (a) is 5.26 Å.

3.5. Morphology analysis

The morphology and size of the ZnS NPs were analyzed by SEM, energy-dispersive X-ray spectroscopy **(EDX)**, TEM and selected area electron diffraction **(SAED)** as shown in Fig. 6*a–d*. The low magnification SEM image (Fig. 6*a*) shows that the ZnS NPs have rough surfaces composed of nanoparticles with an average diameter of about 60 nm which indicates the nanocrystalline nature of the ZnS NPs. The presence of some larger particles is attributed to the aggregation or overlapping of smaller particles. Fig. 6*b* shows the energy-dispersive X-ray spectrum of the fabricated ZnS NPs, confirming the elemental Zn and S signals without peaks from any impurities. Other elemental signals including C, O, and N are possibly due to capping agent present within the Schiff base. The TEM image of the Schiff base capped ZnS NPs is shown in Fig. 6*c*. TEM image of the Schiff base capped ZnS NPs show monodisperse particles with average sizes of 8±2 nm. From TEM image, the synthesized ZnS NPs exhibit nearly spherical shape with a narrow size distribution due to the Schiff base donor atoms interacted with the surface of the NPs. TEM image showed that the ZnS NPs appear a slight agglomeration due to the ZnS was composed of agglomerated and isolated particles and it reveals that small particles aggregate into secondary particles because of their extremely small dimensions and high surface energy. The agglomeration is the most general hurdle in the field of nanoparticles preparation. The SAED pattern of the ZnS NPs showed concentric rings, indicating polycrystalline nature of the material as shown in Fig. 6*d*. These fringes were indexed to (111), (220), and (311) planes of cubic ZnS phase width $d(111) = 3.09$ Å, $d(220) = 1.93$ Å and $d(311) = 1.58$ Å, respectively, confirming the presence of cubic ZnS. These results are corroborated by the XRD pattern of the synthesized ZnS NPs.

3.6. Zeta potential analysis

Zeta potential measurements have been carried out to check the stability of dispersed nanoparticles. Nanoparticles with less than 20 nm diameter have high mobility in solution due to the Brownian motion which highly affects the stability of particles. These electrostatic repulsions between particles depend on the pH. To attain higher zeta potential, nanoparticles should be away from the isoelectric point, therefore the zeta potential values are recorded for optimized pH. The negative zeta potential of ZnS suspensions in aqueous solution changes to positive and negative in the presence of cationic and anionic surfactants, respectively. These transformations in zeta

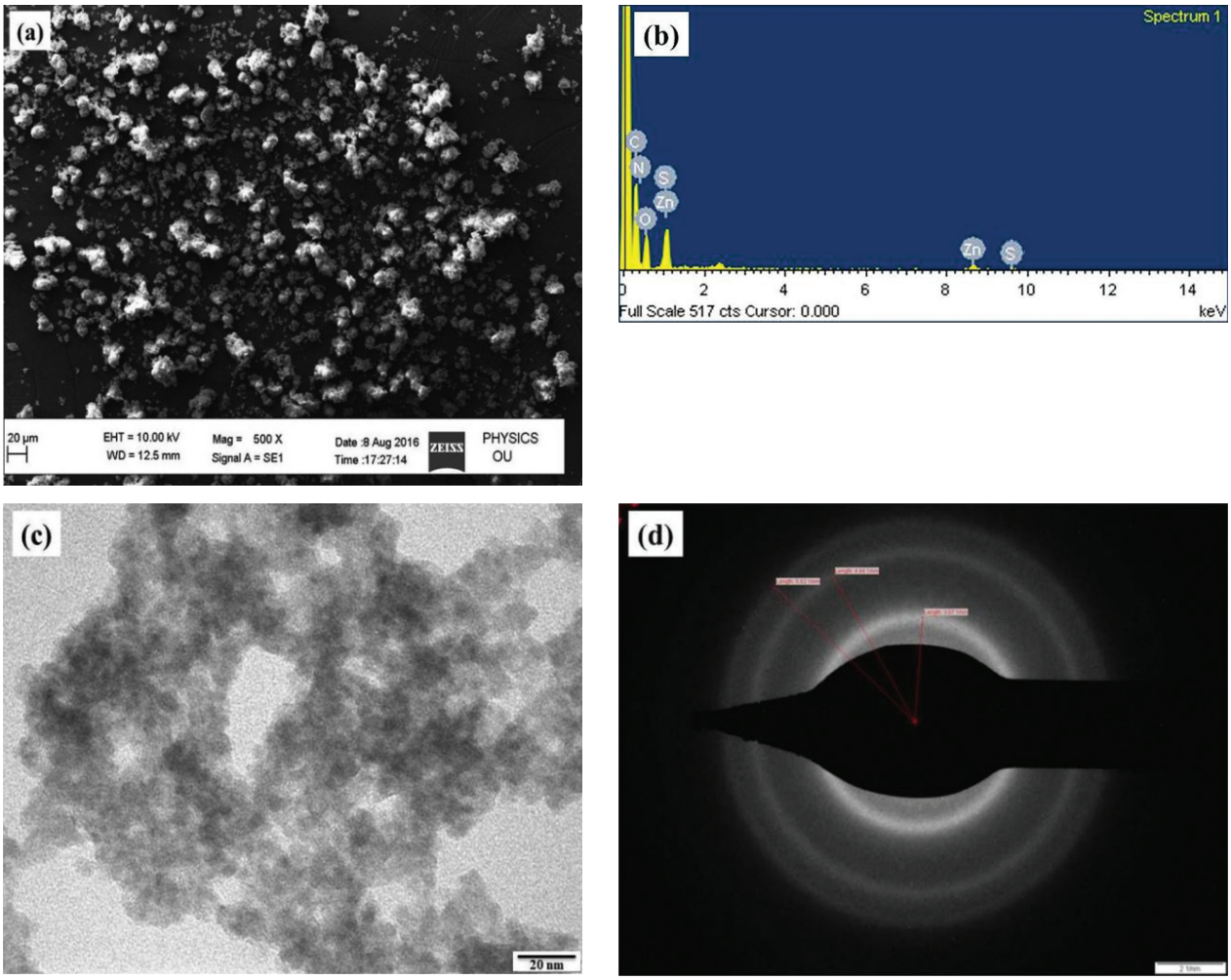

Figure 6. (*a*) SEM mage, (*b*) EDX spectra, (*c*) TEM image and (*d*) SAED of the Schiff base capped ZnS NPs.

potential sign can be crucial in defining the adsorption modes of surfactant aggregates at the NP surface in an aqueous medium. The adsorbed cationic and anionic surfactant aggregates have been thought to generate positively and negatively charged slipping plane respectively, by forming nearly bi-layer structure over the nanoparticle surface. The value of zeta potential for Schiff base capped ZnS NPs at pH 9 is −26.7 mV. These results are on par with zeta potential values of aqueous ZnS suspensions reported by Mehta et al. [51]. It reveals that aqueous suspensions are quite stable because of the electrostatic repulsions between the same charged species.

3.7. Thermo gravimetric analysis

To determine the thermal stability and crystalline conditions of the synthesized Schiff base capped ZnS NPs, thermogravimetry analysis **(TGA)** was investigated as shown in Fig. 7. The sample was heated from room temperature to 800 °C with an increment of 10 °C/min under inert atmosphere. The TGA curve showed some distinct weight losses arising for bare ZnS from desorption of water (below 200 °C), the decomposition of organic species (200–300 °C), the phase transformation of ZnS (300–500 °C), and the above 500 °C, there is a sharp downward trend in TGA curve with significant weight loss; this may be due to release of residual sulfur ions from the sample [52]. ZnS NPs begin to decompose at about 245 °C due to the existence of the unstable Schiff base on ZnS particle surfaces (where the decomposition temperature is defined as 5% weight loss of sample). Notably, in TGA data curve is given in Fig. 7, it is revealed that the weight loss of the ZnS NPs up to 800 °C. The final weight loss was intense with approximately 58.72% mass change. It can be found that the high percentage of weight loss as obtained by TGA is due to the mass of organic molecules capped on the ZnS surface.

3.8. Fluorescence analysis

3.8.1. Fluorescence sensing of heavy metal ions

The fluorescence detection of various aqueous metal ions was performed at room temperature. For an effective sensor, the high selectivity for the target analyte over potentially competitive species is required. Competition

experiments were carried out by recording the changes of the fluorescence intensity before and after adding the metal ions into the probe solution. To test the selectivity of Schiff base capped ZnS NPs for the metal ions; we investigated the fluorometric response in the presence of various metal ions at the concentration of 1 μM. The addition of 10 mL of 1×10^{-6} M of an aqueous solution of Mn^{2+}, Ba^{2+}, Al^{3+}, Cd^{2+}, Cr^{2+}, Cu^{2+}, Fe^{3+}, Ni^{2+}, Co^{2+} and Ag^{+} ions to the ZnS NPs, did not produce significant fluorescence intensity changes. Nevertheless, upon the addition of Fe^{3+}, Cr^{2+} and Cd^{2+} ions to the solution containing ZnS NPs and other metal ions, immediate decrease in fluorescence emission was observed. The fluorescence intensity of probe towards the surveyed metal ions is displayed in Fig. 8*a* and the bar diagram for the selectivity of the sensor among various metal ions was shown in Fig. 8*b*. Therefore, the sensor has a better selectivity for Fe^{3+}, Cr^{2+} and Cd^{2+} ions over other metal ions tested under the similar conditions.

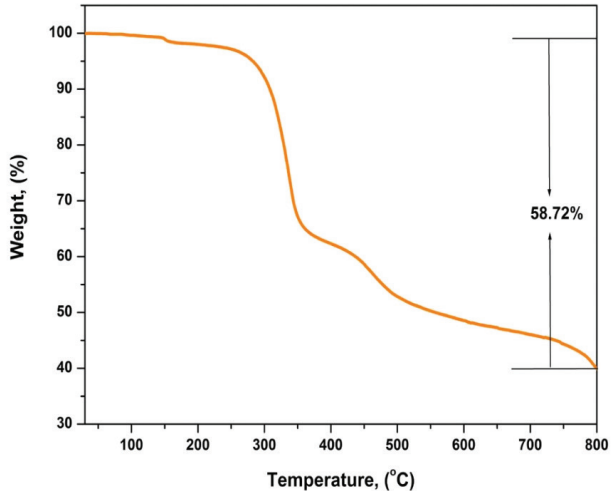

Figure 7. TGA curve of Schiff base capped ZnS NPs.

3.8.2. Fluorescence quenching study

Fluorescence quenching of the ZnS NPs is also strongly affected by the concentration of some metal ions. This phenomenon arises from binding metal ions of interest to the surface of NPs as an acceptor and changing the surface state of NPs, which can be described clearly by the well-known Stern-Volmer equation:

$$\frac{F_0}{F} = 1 + K_{SV}[Q]. \quad (2)$$

Where, F_0 and F are the fluorescence intensity in the absence and presence of the quencher (for example, Fe^{3+} ions), K_{SV} is the Stern-Volmer quenching constant, and Q is the concentration of the quencher. The linear relationship ($R^2 = 0.98$) of the Stern-Volmer plot of F_0/F versus the metal ion concentration suggests that only one type of quencher is available and affects the fluorophore. In other words, the phenomenon of PL quenching can be used for the determination of quencher if a linear regression is found between the concentration of metal ion of interest and PL quenching just according to Stern-Volmer equation. In this case, the slope of the linear relationship is proportional to K_{SV} if the intercept is on level with 1. Evidently, obtaining higher K_{SV} values implies that the measurement is carried out with greater sensitivity. With regards to this criterion, PL quenching of Schiff base capped ZnS NPs was investigated in the presence of several heavy metal ions including Fe^{3+}, Cr^{2+} and Cd^{2+} with different concentrations.

3.8.3. Fluorescence selective probe for detection of Fe^{3+}, Cr^{2+} and Cd^{2+} ions

To understand the interaction between metal ions (Fe^{3+}, $Cr^{2+}$and Cd^{2+}) and ZnS NPs, the response characteristics of nanoparticles to metal ions were systematically studied by fluorescence spectroscopy. As shown in Fig. 9*a–c*, it

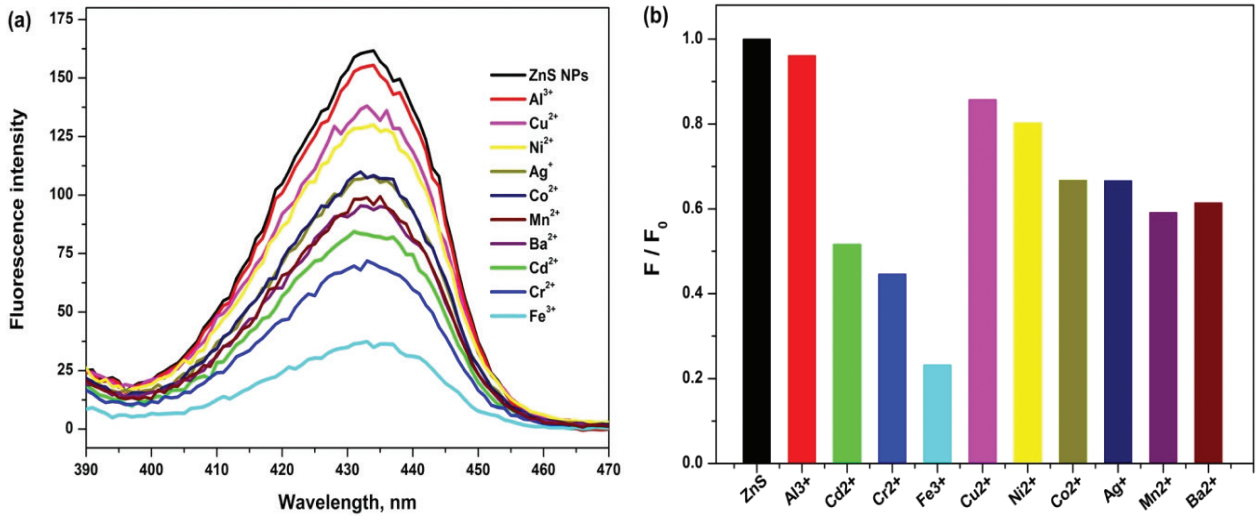

Figure 8. (*a*) fluorescence spectra and (*b*) normalized fluorescence intensity of ZnS NPs alone and in the presence of several different metal ions, λ_{ex} = 340 nm, λ_{em} = 432 nm.

Table 1. Comparison of the previously reported methods with this work in the selective detection of Fe^{3+}, Cr^{2+} and Cd^{2+} ions.

S. No.	Samples	Metal ion	Concentration	Detection limit	Mode of detection	Ref.
1	Carbon NCs	Fe^{3+}	0.01–100 μM	0.001 μM	Fluorometric	[53]
2	B,N,S-co-doped CDs	Fe^{3+}	0.3–546 μM	90 nM	Colorimetric,Fluorometric	[54]
3	Au NPs	Fe^{3+}	0–180 μM	11.3 nM	Colorimetric	[55]
4	Eu^{3+}-Gd_2O_3 NPs	Fe^{3+}	0–10 ppm	1.48 ppm	Fluorometric	[56]
5	Schiff base-ZnS NPs	Fe^{3+}	10–500 μM	10.24 μM	Fluorometric	Present study
6	Au NPs	Cr^{6+}	10–200 nM	0.9 nM	Electrochemical	[57]
7	CdS NPs	Cr^{3+}	0.016–0.260 M	16×10^{-9} M	Fluorometric	[58]
8	Rhodamine based sensor	Cr^{2+}	0.07–3.5 mM	64 μM	Fluorometric	[59]
9	Schiff base-ZnS NPs	Cr^{2+}	10–500 μM	31.48 μM	Fluorometric	Present study
10	Fe_3O_4 NPs	Cd^{2+}	1–15×10–8 M	1.5×10^{-8} M	Fluorometric	[60]
11	MoS_2 NSs	Cd^{2+}	0–11.5 μM	7.2×10^{-8} M	Optical	[61]
12	Ag_2S QDs	Cd^{2+}	0–100 μM	546 nM	Fluorometric	[62]
13	Schiff base-ZnS NPs	Cd^{2+}	10–500 μM	64.56 μM	Fluorometric	Present study

can be seen that a significant fluorescence quenching of ZnS NPs and the emission spectra at 432 nm decreases in the presence of Fe^{3+}, Cr^{2+} and Cd^{2+} ions (10–500 μM) were observed without any significant shift in the emission peak due to the aggregation-induced fluorescence quenching. Therefore, we speculated that the experimental phenomenon can be explained in the terms of strong affinity of these metal ions (Fe^{3+}, Cr^{2+} and Cd^{2+}) to nitrogen atom, which lead to facilitating non-radiative excited electrons (e^-) in the conduction band and holes (h^+) in the valence band recombination on the surface of NPs through an effective electron transfer process between surface functional imine group and metal ions (Fe^{3+}, Cr^{2+} and Cd^{2+}). In the stage of when 500 μM of Fe^{3+} was added to the NPs solution, the fluorescence intensity of ZnS NPs at 432 nm decreased by about 85%. Similarly, when 500 μM of Cr^{2+} and Cd^{2+} were added separately into the ZnS solution, the fluorescence intensity of ZnS NPs at 432 nm decreased by about 62% and 41%, respectively. This indicates that the reaction between the surface functional groups of Schiff base capped ZnS NPs and Fe^{3+} is very fast and stable, suggesting a promising application for quick sensing of Fe^{3+} without any strict time control than Cr^{2+} and Cd^{2+} ions. These results revealed the excellent selection of the ZnS NPs as a fluorescence probe for Fe^{3+} detection as well as Cr^{2+} and Cd^{2+} ions compared to other metal ions.

The bar diagram of the different concentrations (10–100 μM) of these metal ions (Fe^{3+}, Cr^{2+} and Cd^{2+}) shows that the fluorescence intensity of ZnS NPs as a concentration dependent and it was shown in Fig. 9*d*. The titration of different concentrations of these metal ions (Fe^{3+}, Cr^{2+} and Cd^{2+}) into the ZnS NPs solution resulted in a gradual decrease in fluorescence intensity with increasing concentration of metal ions in the range of 10–500 μM (Fig. 9*e*). Fig. 9*f* shows the linear responses of the fluorescence intensity (F_0/F) with the increasing concentration of these metal ions (Fe^{3+}, Cr^{2+} and Cd^{2+}) in the range of 10–100 μM, showing a correlation coefficient of 0.98. From the quenching study, the corresponding K_{SV} values for the metal ions conformed to Eq. (2) in the presence of Fe^{3+}, Cr^{2+} and Cd^{2+} were 3.64×10^5, 3.11×10^5 and 2.55×10^5 respectively. The obtained selective sensing in the detection of metal ions in the range of detection limit values were 10.24 μM, 31.48 μM and 64.56 μM for Fe^{3+}, Cr^{2+} and Cd^{2+} ions, respectively. The variations were associated with the nature of binding between the metal ions and synthesized Schiff base capped ZnS NPs. The comparison of the previously reported methods, the concentration range of corresponding metal ions and their detection limits with this work in the selective detection of Fe^{3+}, Cr^{2+} and Cd^{2+} ions were listed in Table 1.

4. Conclusions

In summary, we report a simple method to fabricate and stabilize ZnS NPs using Schiff base by co-precipitation method. HR-TEM analysis showed that the synthesized NPs were less than 10 nm in size. The cubic phase of synthesized Schiff base capped ZnS NPs was observed from the XRD. The optical properties of the ZnS NPs were investigated by UV–vis DRS and PL spectroscopy. The obtained ZnS NPs showed a band gap of 3.98 eV, which is in agreement with published literature for cubic zinc blende structure. The interactions among ZnS NPs and metal ions were investigated using fluorescence studies. Under optimal conditions, the developed sensor was successfully employed to determine Fe^{3+}, Cr^{2+} and Cd^{2+} ions in real samples and proved to be selective and as well as sensitive. The ZnS NPs exhibited good fluorescence quenching selectivity to Fe^{3+}, Cr^{2+} and Cd^{2+} ions. Concentration experiments showed that there existed two parts of a linear relationship between fluorescence intensity and concentration of Fe^{3+}, Cr^{2+} and Cd^{2+} ions in the range of 10–500 μM. The limit of detection (LOD) was estimated to be 10.24 μM, 31.48 μM and 64.56 μM for Fe^{3+}, Cr^{2+} and Cd^{2+} ions, respectively. The output of this study clearly suggests that synthesized Schiff base capped ZnS NPs can be used as a promising nanomaterial for efficient fluorescent material for quenching and sensing applications.

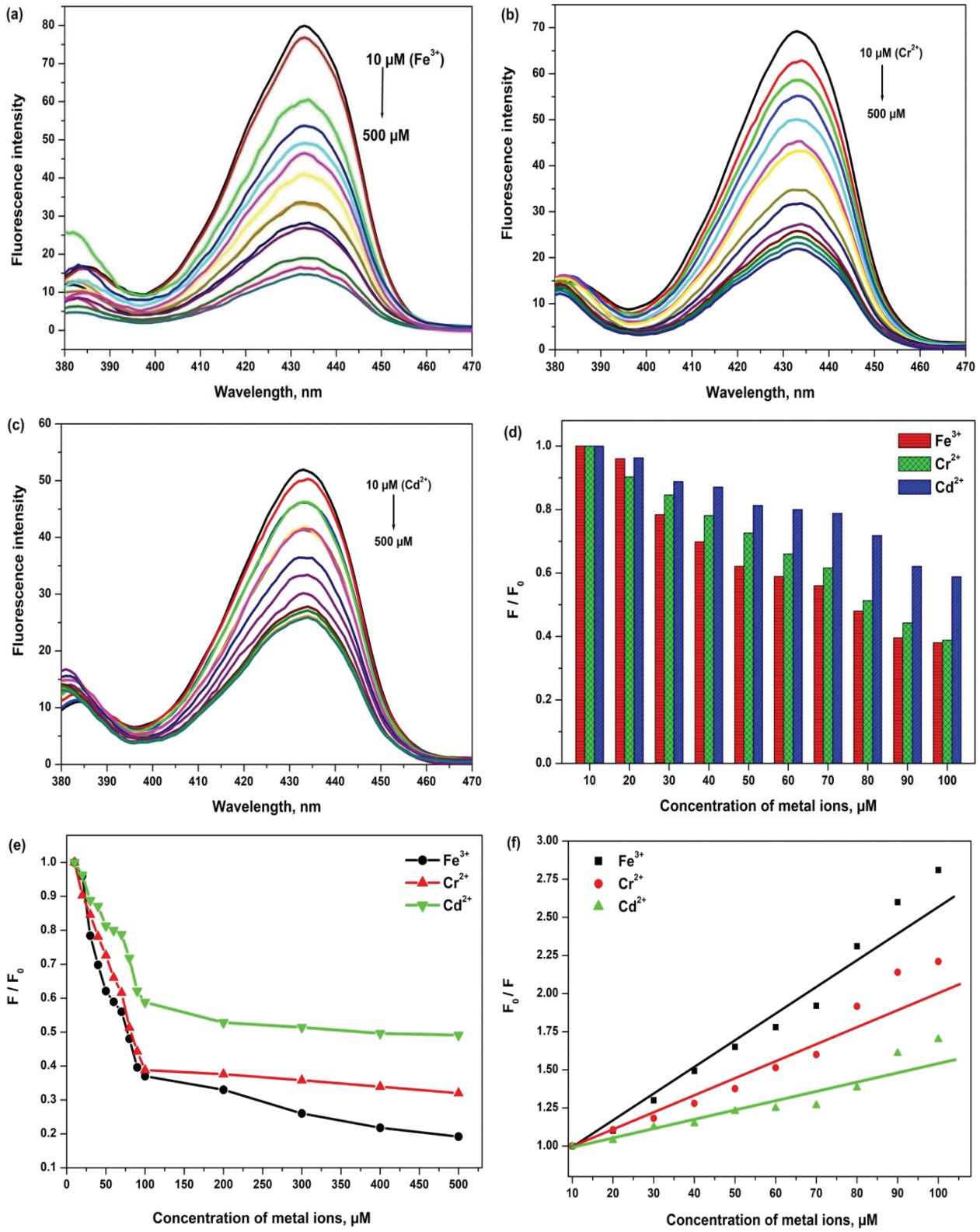

Figure 9. The fluorescence response of Schiff base capped ZnS NPs; in the presence of carious concentrations of (*a*) Fe^{3+}, (*b*) Cr^{2+} and (*c*) Cd^{2+} ions; (*d*) bar diagram of the effect of Fe^{3+}, Cr^{2+} and Cd^{2+} concentrations (10 to 100 μM) in the ZnS fluorescence intensity; (*e*) the relationship between relative concentrations (10 to 500 μM) of Fe^{3+}, Cr^{2+} and Cd^{2+} with ZnS fluorescence intensity; (*f*) the relation between fluorescence response (F_0/F) of ZnS NPs and the concentration of Fe^{3+}, Cr^{2+} and Cd^{2+} from 10 to 100 μM.

Acknowledgements

The authors would like to acknowledge the Head, Department of Chemistry, Osmania University for providing the necessary facilities. One of the authors, D. Ayodhya wishes to thank the UGC, New Delhi which supported this work. The authors would like to thank DST-FIST, New Delhi, India for providing necessary analytical facilities in the department.

References

1. Khalkhali M., Liu Q., Zeng H., Zhang H. A size-dependent structural evolution of ZnS nanoparticles. *Sci. Rep.* 2015; 5: 14267. https://doi.org/10.1038/srep14267
2. Bhadra R., Singh V.N., Mehta B.R., Datta P. Studies on some aspects of ZnS nanocrystals for possible applications in electronics. *Chalcogenide Lett.* 2009; 6(5): 189–196. http://chalcogen.ro/189_Bhadra-Singh-Mehta.pdf
3. Ayodhya D., Venkatesham M., Kumari A.S., Reddy G.B., Ramakrishna D., Veerabhadram G. Synthesis, characterization, fluorescence, photocatalytic and antibacterial activity of CdS nanoparticles using Schiff base. *J. Fluoresce*. 2015; 25(5): 1481–1492. https://doi.org/10.1007/s10895-015-1639-5
4. Ayodhya D., Veerabhadram G. Investigation of structural, optical, catalytic, fluorescence studies of eco-friendly synthesized Bi_2S_3 nanostructures. *Superlattices and Microstructures*. 2017; 102: 103–118. https://doi.org/10.1016/j.spmi.2016.12.027
5. Ayodhya D., Veerabhadram G. Green synthesis, characterization, photocatalytic, fluorescence and antimicrobial activities of Cochlospermum gossypium capped Ag_2S nanoparticles. *J. Photochem. Photobio. B: Biology*. 2016; 157: 57–69. https://doi.org/10.1016/j.jphotobiol.2016.02.002
6. Ayodhya D., Venkatesham M., Kumari A.S., Reddy G.B., Ramakrishna D., Veerabhadram G. Photocatalytic degradation of dye pollutants under solar, visible and UV lights using green synthesised CuS nanoparticles. *J. Exp. Nanosci.* 2016; 11(6): 418–432. https://doi.org/10.1080/17458080.2015.1070312
7. Emadi H., Salavati-Niasari M., Sobhani A. Synthesis of some transition metal (M: $_{25}$Mn, $_{27}$Co, $_{28}$Ni, $_{29}$Cu, $_{30}$Zn, $_{47}$Ag, $_{48}$Cd) sulfide nanostructures by hydrothermal method. *Advances in Colloid and Interface Science*. 2017; 246: 52–74. https://doi.org/10.1016/j.cis.2017.06.007
8. Ghanbari D., Salavati-Niasari M. Synthesis of urchin-like CdS-Fe_3O_4 nanocomposite and its application in flame retardancy of magnetic cellulose acetate. *J. Indus. Eng. Chem.* 2015; 24: 284–292. https://doi.org/10.1016/j.jiec.2014.09.043
9. Mousavi-Kamazani M., Salavati-Niasari M., Goudarzi M., Zarghami Z. Hydrothermal synthesis of $CdIn_2S_4$ nanostructures using new starting reagent for elevating solar cells efficiency. *J. Molecular Liquids.* 2017; 242: 653–661. https://doi.org/10.1016/j.molliq.2017.07.059
10. Mousavi-Kamazani M., Zarghami Z., Salavati-Niasari M. Facile and novel chemical synthesis, characterization, and formation mechanism of copper sulfide (Cu_2S, Cu_2S/CuS, CuS) nanostructures for increasing the efficiency of solar cells. *J. Phys. Chem. C.* 2016; 120(4): 2096–2108. https://doi.org/10.1021/acs.jpcc.5b11566
11. Sabet M., Salavati-Niasari M., Amiri O. Using different chemical methods for deposition of CdS on TiO_2 surface and investigation of their influences on the dye-sensitized solar cell performance. *Electrochimica Acta*. 2014; 117: 504–520. https://doi.org/10.1016/j.electacta.2013.11.176
12. Safardoust-Hojaghan H., Shakouri-Arani M., Salavati-Niasari M. Structural and spectroscopic characterization of HgS nanoparticles prepared via simple microwave approach in presence of novel sulfuring agent. *Transactions of Nonferrous Metals Society of China*. 2016; 26(3): 759–766. https://doi.org/10.1016/S1003-6326(16)64166-3
13. Ayodhya D., Veerabhadram G. Hydrothermally generated and highly efficient sunlight responsive SiO_2 and TiO_2 capped Ag_2S nanocomposites for photocatalytic degradation of organic dyes. *J. Environ. Chem. Eng*. 2018; 6: 311–324. https://doi.org/10.1016/j.jece.2017.11.071
14. Yi R., Qiu G., Liu X. Rational synthetic strategy: From ZnO nanorods to ZnS nanotubes. *J. Solid State Chem*. 2009; 182: 2791–2795. https://doi.org/10.1016/j.jssc.2009.07.038
15. Kaur M., Gupta N.K., Nagaraja C.M. One-pot, template-free syntheses of spherical ZnS nanocrystals using a new S^{2-} source and their photocatalytic study. *Cryst. Eng. Comm*. 2015; 17: 2359–2367. https://doi.org/10.1039/C4CE02556C
16. Rajabi H.R. Shamsipur M. Khosravi A.A. Khani O., Yousefi M.H. Selective spectrofluorimetric determination of sulfide ion using manganese doped ZnS quantum dots as luminescent probe. *Spectrochimica Acta Part A: Molecular and Biomolecular Spectroscopy*. 2013; 107: 256–262. https://doi.org/10.1016/j.saa.2013.01.045
17. Shamsipur M., Rajabi H.R. Pure zinc sulfide quantum dot as highly selective luminescent probe for determination of hazardous cyanide ion. *Mater. Sci. Eng. C*. 2014; 36: 139–145. https://doi.org/10.1016/j.msec.2013.12.001
18. La Porta F.A., Ferrer M.M., De Santana Y.V., Raubach C.W., Longo V.M., Sambrano J.R., Longo E., Andres J., Li M.S., Varela J.A. Synthesis of wurtzite ZnS nanoparticles using the microwave assisted solvothermal method. *J. Alloy. Compd*. 2013; 556: 153–159. https://doi.org/10.1016/j.jallcom.2012.12.081
19. Zhu J., Zhou M., Xu J., Liao X. Preparation of CdS and ZnS nanoparticles using microwave irradiation. *Mater. Lett.* 2001; 47: 25–29. https://doi.org/10.1016/S0167-577X(00)00206-8
20. Khiew P.S., Radiman S., Huang N.M., Ahmed S.M., Nadarajah K. Preparation and characterization of ZnS nanoparticles synthesized from chitosan laurate micellar solution. *Mater. Lett.* 2005; 59: 989–993. https://doi.org/10.1016/j.matlet.2004.11.044
21. Bessergenev V.G., Ivanova E.N., Kovalevskaya Y.A., Gromilov S.A., Kirichenko V.N., Zemskova S.M., Vasilieva I.G., Ayupov B.M., Shwarz N.L. Optical and structural proper tees of ZnS and ZnS:Mn films prepared by CVD method. *Mater. Res. Bull.* 1995; 30: 1393–1400. https://doi.org/10.1016/0025-5408(95)00150-6
22. Ayodhya D., Venkatesham M., Kumari A.S., Mangatayaru K.G., Veerabhadram G. Synthesis, characterization of ZnS nanoparticles

by coprecipitation method using various capping agents-photocatalytic activity and kinetic study. *J. Appl. Chem*. 2013; 6(1): 1–9. https://doi.org/10.9790/5736-0610109

23. Liu J., Ma J., Liu Y., Song Z., Sun Y., Fang J., Liu Z. Synthesis of ZnS nanoparticles via hydrothermal process assisted by microemulsion technique. *J. Alloys Compd.* 2009; 486: L40–L43. https://doi.org/10.1016/j.jallcom.2009.07.109
24. Denzler D., Olschewski M., Sattler K. Luminescence studies of localized gap states in colloidal ZnS nanocrystals. *J. Appl. Phys*. 1998; 84: 2841–2845. https://doi.org/10.1063/1.368425
25. Sasakura H., Kobayashi H., Tanaka S., Mita J., Tanaka T., Nakayama H. The dependences of electroluminescent characteristics of ZnS:Mn thin films upon their device parameters. *J. Appl. Phys*. 1981; 52: 6901–6906. https://doi.org/10.1063/1.328642
26. Huang J., Yang Y., Xue S., Yang B., Liu S., Shen J. Photoluminescence and electroluminescence of ZnS:Cu nanocrystals in polymeric networks. *Appl. Phys. Lett*. 1997; 70: 2335–2337. https://doi.org/10.1063/1.118866
27. Sharma R., Bisen D.P. Thermoluminescence of mercaptoethanol-capped ZnS:Mn nanoparticles. *Luminescence*. 2015; 30(2): 175–181. https://doi.org/10.1002/bio.2710
28. Frankl D.R. Electroluminescence of ZnS single crystals with cathode barriers. *Phys. Rev*. 1958; 111: 1540–1549. https://doi.org/10.1103/PhysRev.111.1540
29. Chen W., Wang Z., Lin Z., Lin L. Absorption and luminescence of the surface states in ZnS nanoparticle. *J. Appl. Phys*. 1997; 82: 3111–3115. https://doi.org/10.1063/1.366152
30. Ayodhya D., Veerabhadram G., One-pot green synthesis, characterization, photocatalytic, sensing and antimicrobial studies of Calotropis gigantea leaf extract capped CdS NPs. *Mater. Sci. Eng. B*. 2017; 225: 33–44. https://doi.org/10.1016/j.mseb.2017.08.008
31. Rurack K., Genger U.R. Rigidization, preorientation and electronic decoupling-the 'magic triangle' for the design of highly efficient fluorescent sensors and switches. *Chem. Soc. Rev.* 2002; 31: 116–127. https://doi.org/10.1039/b100604p
32. Huber J.K. Determination of Cu, Fe, Mn, and Zn in blood fractions by SEC-HPLC-ICP-AES coupling. *Analyst*. 1999; 124(5): 657–663. https://doi.org/10.1039/a809688k
33. del Castillo Busto M.E., Montes-Bayón M., Blanco-González E., Meija J., Sanz-Medel A. Strategies to study human serum transferrin isoforms using integrated liquid chromatography ICPMS, MALDI-TOF, and ESI-Q-TOF detection: application to chronic alcohol abuse. *Anal. Chem.* 2005; 77(17): 5615–5621. https://doi.org/10.1021/ac050574s
34. Andersen J.E. A novel method for the filterless preconcentration of iron. *Analyst*. 2005; 130: 385–390. https://doi.org/10.1039/b412061b
35. van den Berg C.M.G. Chemical speciation of iron in seawater by cathodic stripping voltammetry with dihydroxy naphthalene. *Anal. Chem.* 2006; 78(1): 156–163. https://doi.org/10.1021/ac051441
36. Dilgin Y., Kizilkaya B., Ertek B., Eren N., Dilgin D.G. Amperometric determination of sulfide based on its electrocatalytic oxidation at a pencil graphite electrode modified with quercetin. *Talanta*. 2012; 89: 490–495. https://doi.org/10.1016/j.talanta.2011.12.074
37. Radford-Knoery J., Cutter G.A. Determination of carbonyl sulfide and hydrogen sulfide species in natural waters using specialized collection procedures and gas chromatography with flame photometric detection. *Anal. Chem*. 1993; 65: 976–982. https://doi.org/10.1021/ac00056a005
38. Safavi A., Karimi M.A. Flow injection chemiluminescence determination of sulfide by oxidation with N-bromo succinimide and N-chloro succinimide. *Talanta*. 2002; 57: 491–500. https://doi.org/10.1016/S0039-9140(02)00048-6
39. Ghasemi J., Ebrahimi D.M., Hejazi L., Leardi R., Niazi A. Simultaneous kinetic-spectrophotometric determination of sulfide and sulfite by partial least squares and genetic algorithm variable selection. *J. Anal. Chem*. 2007; 62: 348–354. https://doi.org/10.1134/S1061934807040090
40. Ayodhya D., Veerabhadram G. Preparation, characterization, photocatalytic, sensing and antimicrobial Studies of Calotropis gigantea leaf extract capped CuS NPs by a green approach. *J. Inorg. Organomet. Polymer Mat*. 2017; 27: 215–230. https://doi.org/10.1007/s10904-017-0672-z
41. Mishra A.P., Soni M. Synthesis, structural, and biological studies of some Schiff bases and their metal complexes. *Met. Based Drugs*. 2008; 2008: 875410. https://doi.org/10.1155/2008/875410
42. Shreenivas M.T., Chetan B.P., Bhat A.R. Synthesis and pharmacological evaluation of certain Schiff bases and thiazoldine derivatives as AT1 Angiotension-II (AII) receptor Antagonists. *J. Pharm. Sci. Tech.* 2009; 1: 88–94.
43. Kumar S., Dhar D.N., Saxena P.N. Applications of metal complexes of Schiff bases-A review. *J. Scientific and Industrial Research*. 2009; 68(3): 181–187.
44. Forzani E.S., Foley K., Westerhoff P., Tao N. Detection of arsenic in groundwater using a surface plasmon resonance sensor. *Sensors and Actuators B: Chem*. 2007; 123(1): 82–88. https://doi.org/10.1016/j.snb.2006.07.033
45. Reddy D.A., Liu C., Vijayalakshmi R.P., Reddy B.K. Effect of Al doping on the structural, optical and photoluminescence properties of ZnS nanoparticles. *J. Alloys Compd*. 2014; 582: 257–264. https://doi.org/10.1016/j.jallcom.2013.08.051
46. Mehta S.K., Kumar S., Chaudhary S., Bhasin K.K. Effect of cationic surfactant head groups on synthesis, growth and agglomeration behavior of ZnS nanoparticles. *Nanoscale Res. Lett.* 2009; 4: 1197–1208. https://doi.org/10.1007/s11671-009-9377-8
47. Naeimi H., Foroughi H. Facile three-component preparation of benzodiazepine derivatives catalyzed by zinc sulfide nanoparticles via grinding method. *Res. Chem. Intermed*. 2016; 42: 3999–4020. https://doi.org/10.1007/s11164-015-2254-4
48. Sapra S., Prakash A., Ghangrekar A., Periasamy N., Sarma D.D. Emission properties of manganese-doped ZnS nanocrystals. *J. Phys. Chem. B.* 2005; 109: 1663–1668. https://doi.org/10.1021/jp049976e
49. Mala J.G.S., Rose C. Facile production of ZnS quantum dot nanoparticles by Saccharomyces cerevisiae MTCC 2918. *J. Biotechnol*. 2014; 170: 73–78. https://doi.org/10.1016/j.jbiotec.2013.11.017
50. Frasco M.F., Chaniotakis N. Semiconductor quantum dots in chemical sensors and biosensors. *Sensors*. 2009; 9(9): 7266–7286. https://doi.org/10.3390/s90907266
51. Mehta S.K., Kumar S., Gradzielski M. Growth, stability, optical and photoluminescent properties of aqueous colloidal ZnS nanoparticles in relation to surfactant molecular structure. *J. Colloid Interface Sci.* 2011; 360: 497–507. https://doi.org/10.1016/j.jcis.2011.04.079
52. Kuppayee M., Nachiyar G.K.V., Ramasamy V. Synthesis and characterization of Cu^{2+} doped ZnS nanoparticles using TOPO and SHMP as capping agents. *Appl. Surf. Sci.* 2011; 257: 6779–6786. https://doi.org/10.1016/j.apsusc.2011.02.124
53. Bhamore J.R., Jha S., Singhal R.K., Kailasa S.K. Synthesis of water dispersible fluorescent carbon nanocrystals from syzygium cumini

fruits for the detection of Fe^{3+} ion in water and biological samples and imaging of Fusarium avenaceum cells. *J. Fluoresc*. 2017; 27: 125–134. https://doi.org/10.1007/s10895-016-1940-y

54. Liu Y., Duan W., Song W., Liu J., Ren C., Wu J., Liu D., Chen H. Dual-colored carbon dot ratiometric fluorescent test paper based on a specific spectral energy transfer for semi-quantitative assay of copper ions. *ACS Appl. Mater. Interfaces*. 2017; 9(22): 18897–18903. https://doi.org/10.1021/acsami.7b05827
55. Kim K., Nam Y.S., Lee Y., Lee K.B. Highly sensitive colorimetric assay for determining Fe^{3+} based on gold nanoparticles conjugated with glycol chitosan. *J. Analyt. Methods in Chem*. 2017; 2017: 3648564. https://doi.org/10.1155/2017/3648564
56. Chaudhary S., Kumar S., Umar A., Singh J., Rawat M., Mehta S.K. Europium-doped gadolinium oxide nanoparticles: A potential photoluminescencent probe for highly selective and sensitive detection of Fe^{3+} and Cr^{3+} ions. *Sensors and Actuators B.* 2017; 243: 579–588. https://doi.org/10.1016/j.snb.2016.12.002
57. Tan F., Cong L., Jiang X., Wang Y., Quan X., Chen J., Mulchandani A. Highly sensitive detection of Cr(VI) by reduced graphene oxide chemiresistor and 1,4-dithiothreitol functionalized Au nanoparticles. *Sensors and Actuators B.* 2017; 247: 265–272. https://doi.org/10.1016/j.snb.2017.02.163
58. Ahmed K.B.A., Pichikannu A., Veerappan A. Fluorescence cadmium sulfide nanosensor for selective recognition of chromium ions in aqueous solution at wide pH range. *Sensors and Actuators B.* 2015; 221: 1055–1061. https://doi.org/10.1016/j.snb.2015.07.035
59. Rull-Barrull J., d'Halluin M., Le Grognec E., Felpin F.X. A highly selective colorimetric and fluorescent chemosensor for Cr^{2+} in aqueous solutions. *Tetrahedron Lett.* 2017; 58: 505–508. https://doi.org/10.1016/j.tetlet.2016.12.038
60. Wang M., Meng G., Huang Q., Lu Y., Gu Y. Fluorophore-modified Fe_3O_4-magnetic-nanoparticles for determination of heavy metal ions in water. *Sensors and Actuators B.* 2013; 185: 47–52. https://doi.org/10.1016/j.snb.2013.04.086
61. Yin W., Dong X., Yu J., Pan J., Yao Z., Gu Z., Zhao Y. MoS_2-nanosheet-assisted coordination of metal ions with porphyrin for rapid detection and removal of cadmium ions in aqueous media. *ACS Appl. Mater. Interfaces*. 2017; 9(25): 21362–21370. https://doi.org/10.1021/acsami.7b04185
62. Wu Q., Zhou M., Shi J., Li Q., Yang M., Zhang Z. Synthesis of water-soluble Ag_2S quantum dots with fluorescence in the second near-infrared window for turn-on detection of Zn(II) and Cd(II). *Anal. Chem.* 2017; 89: 6616–6623. https://doi.org/10.1021/acs.analchem.7b00777